Ideal Cluster Research Material

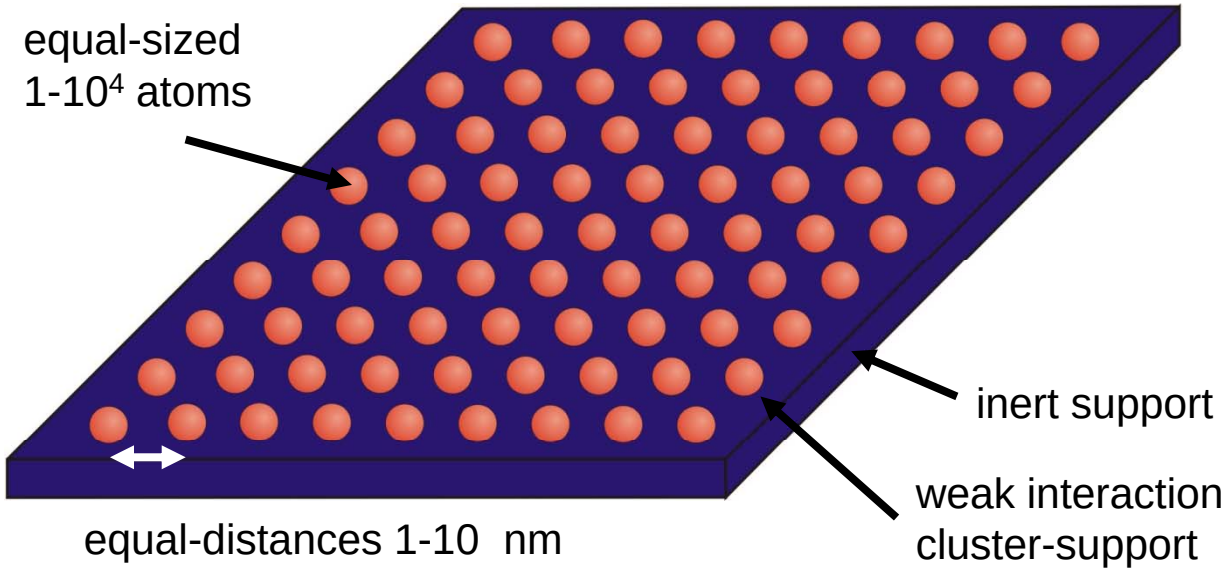

- address single clusters
- collective cluster response
- cluster coupling

Fig. 5.16

Deposition of Mass-Selected Clusters

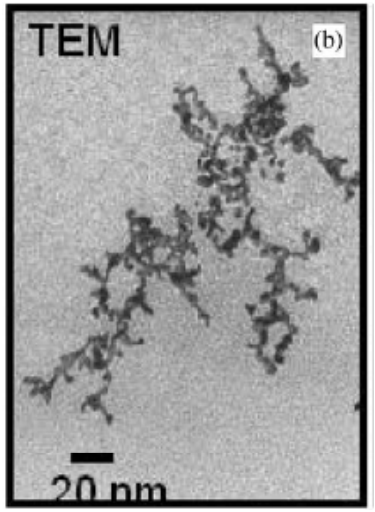

Pt-clusters, 0.25 eV/atom
→ aggregation [1]

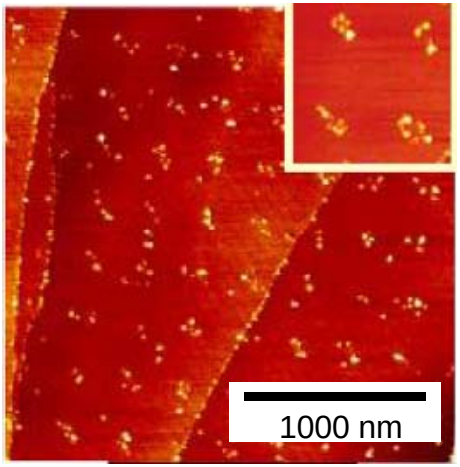

FIB-prepatterned,
then Au_{750}
0.25 eV/atom [1]

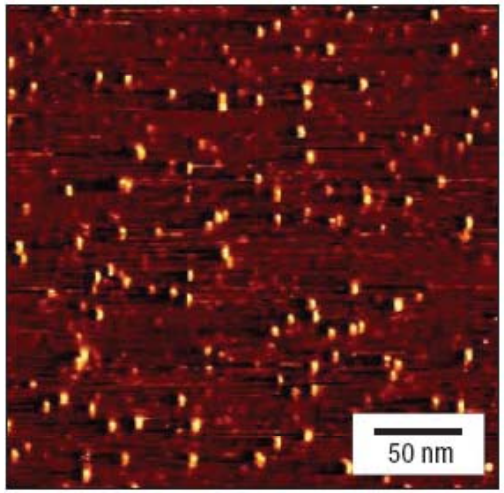

Ag_{147}, 14 eV/atom [2]

Fig. 5.17

[1] P. Mélinon et al., J. Crys. Growth 275 (2005) 317,
[2] R.E. Palmer, S. Pratontep, H.-G. Boyen, Nature Materials 2 (2003) 443

Ir-Clusters on Graphene on Ir(111)

4 atoms/cluster

9 atoms/cluster

250 Å

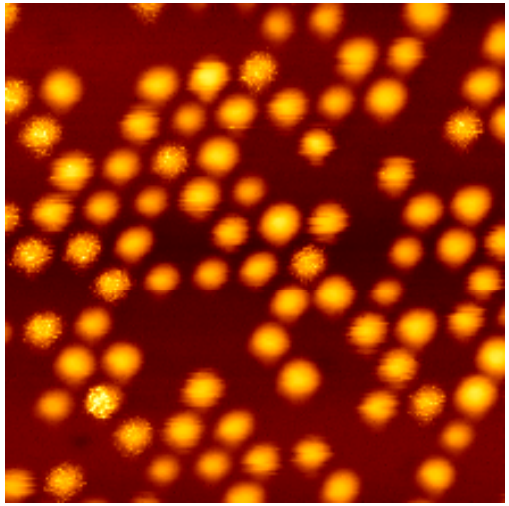

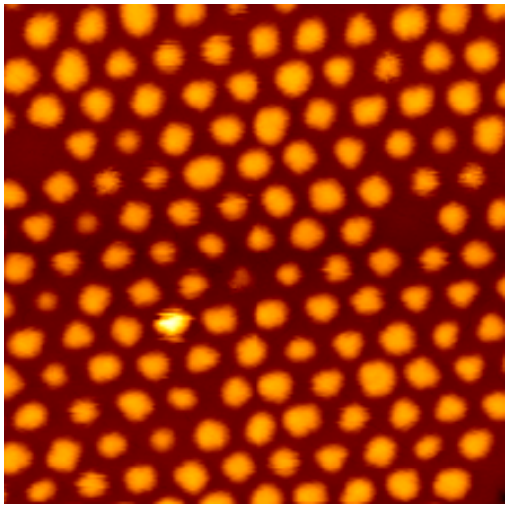

70 atoms/cluster

130 atoms/cluster

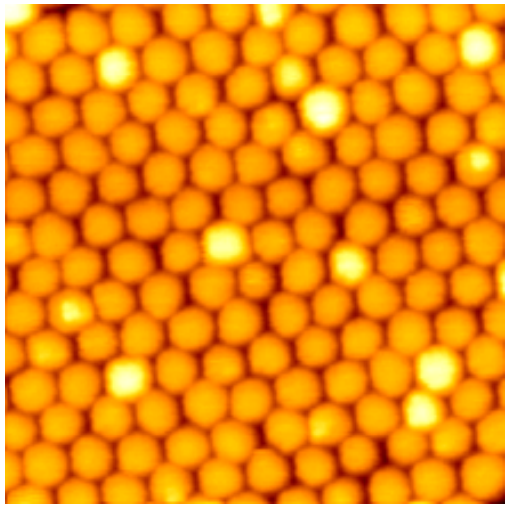

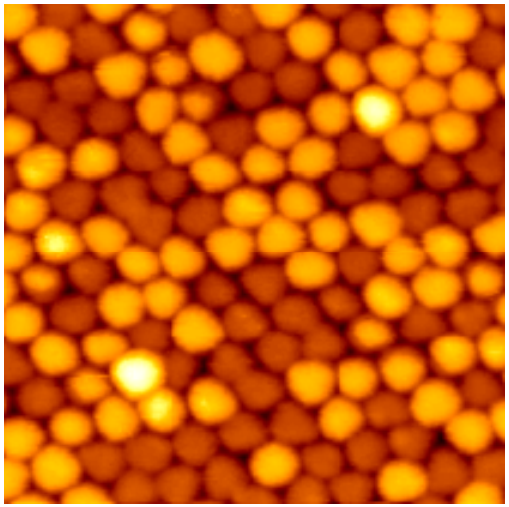

substrate:
graphene moiré on Ir(111)

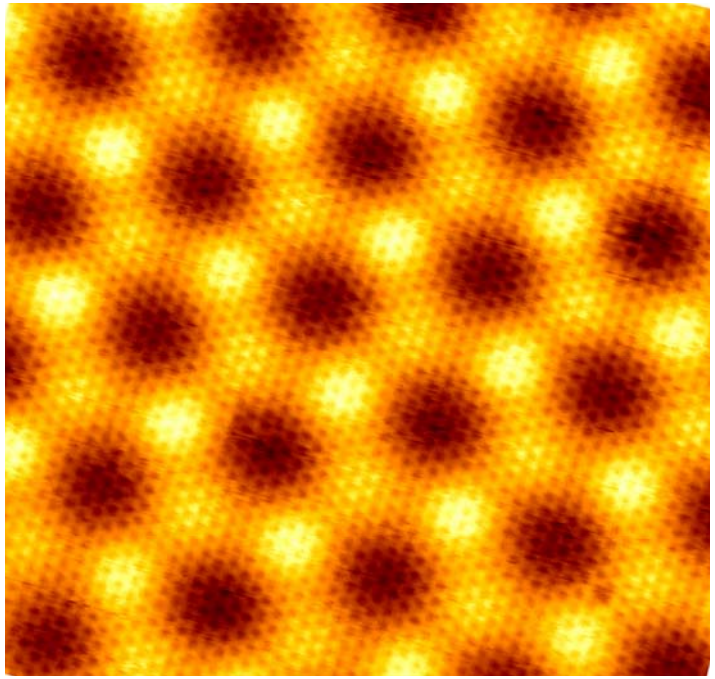

100 Å

Fig. 5.18

A. N'Diaye. S. Bleikamp, P.J. Feibelman, T. Michely, Phys. Rev. Lett. 97 (2006) 215501

Origin of Moiré

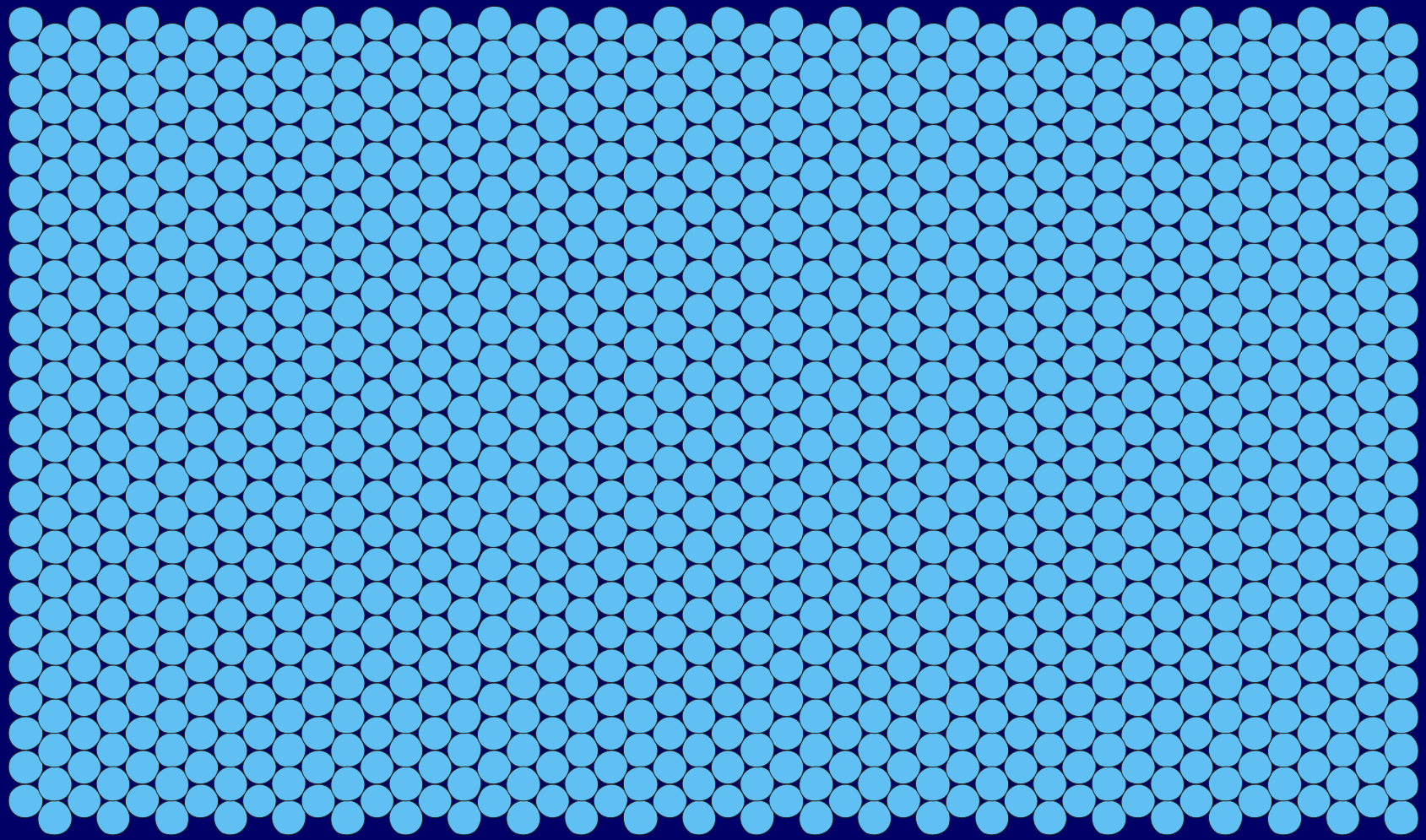

Ir(111)

Fig. 5.19

Origin of Moiré

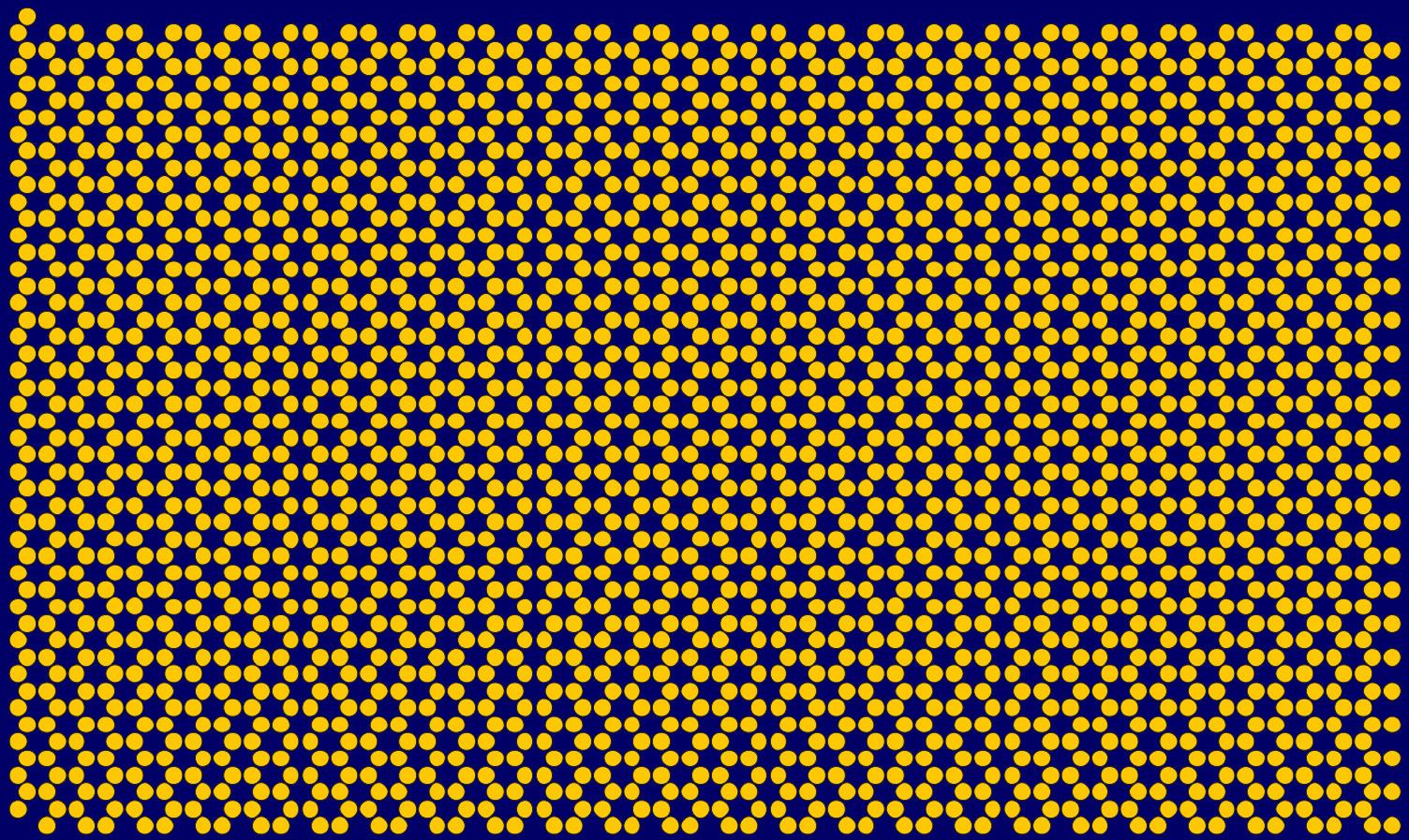

graphene

Fig. 5.20

Origin of Moiré

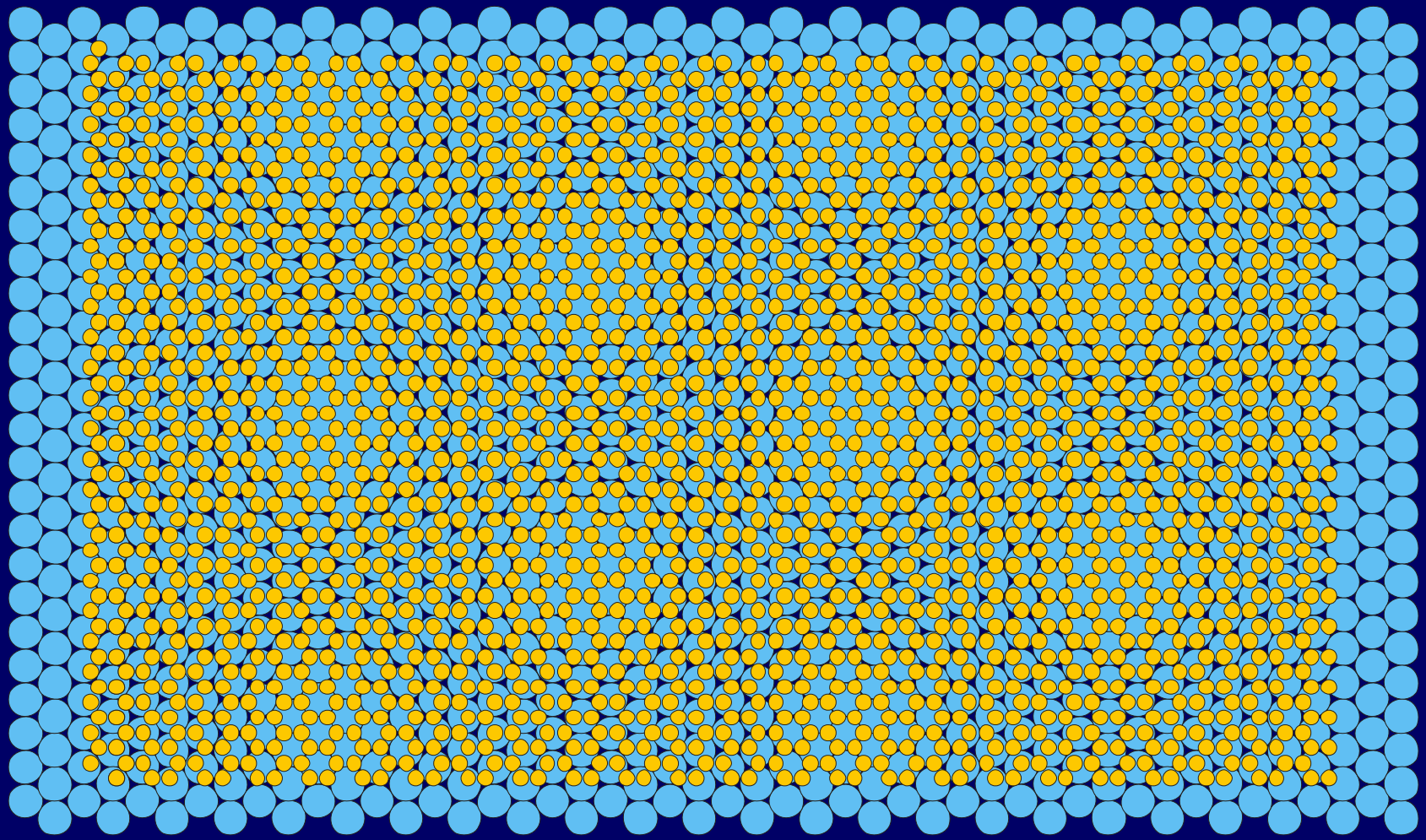

Ir(111) and graphene

Fig. 5.21

DFT-calculations: Pinning Effect

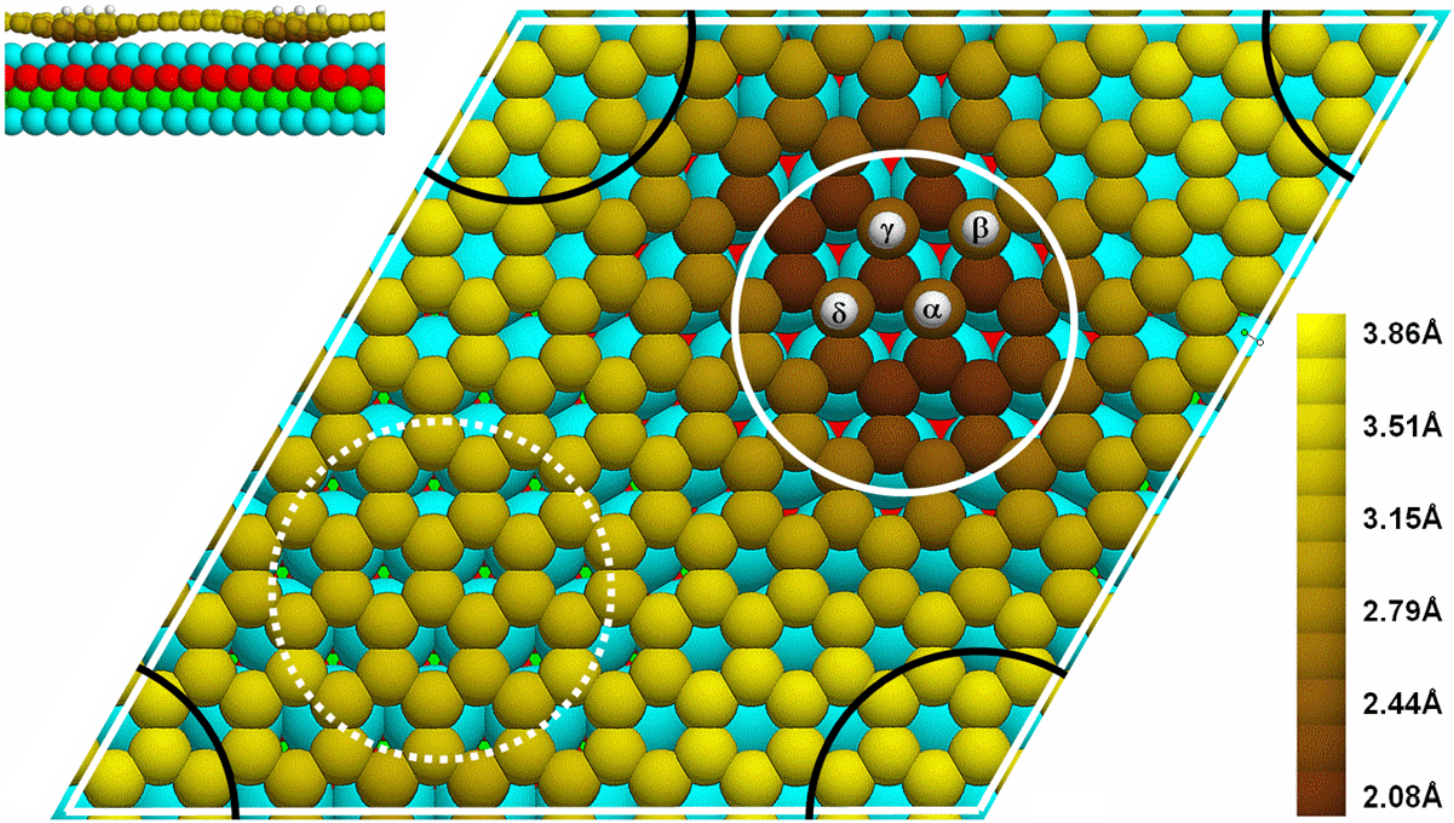

- short bonds ≈ 2.1 Å ≈ sum of Ir and C atomic radii
- more than twice C-Ir chemical bonds than adatoms !

Fig. 22

- hcp-type prefered by 3.7 eV

Nano-Diamond Formation Underneath Cluster

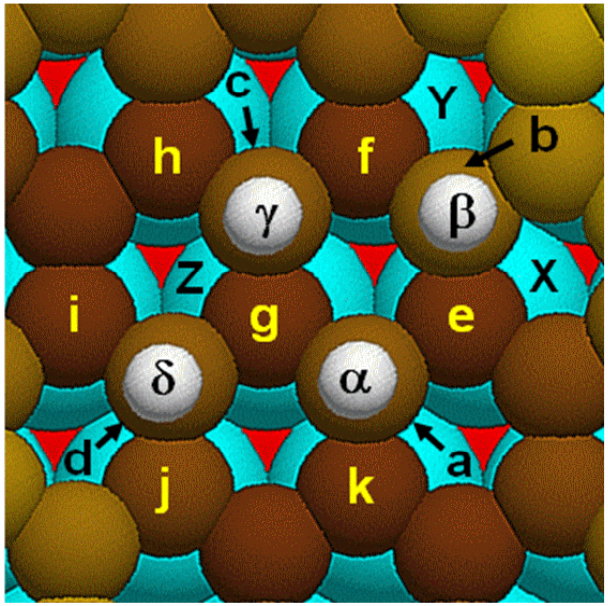

bond angles:

Xea, Xeb, Yfb, Yfc, Zgc, Zgd, Zga = 111°, 107°, 107°, 110°, 107°, 109°, 108°
eaα, ebβ, fbβ, fcγ,gcγ, gdγ, gdδ,gdα = 106°,108°,108°,105°,106°,111°,106°

Fig. 5.23

tetrahedral bond angle 109,5° rehybridzation from sp^2 to sp^3

P.J. Feibelman, Phys. Rev. B 77 (2008) 165419

Cluster Lattices of Pt, Re, W, Ir

Pt, s_{av} = 25 atoms, 350 K

750 Å

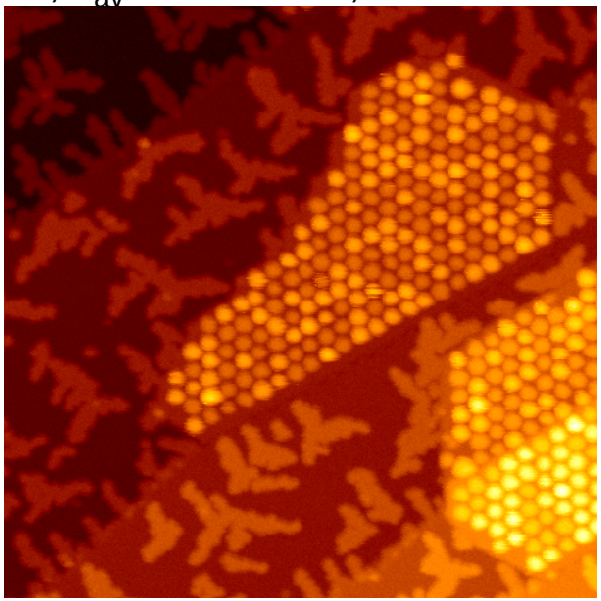

W, $8 \leq s_{av} \leq 16$ atoms, 310 K

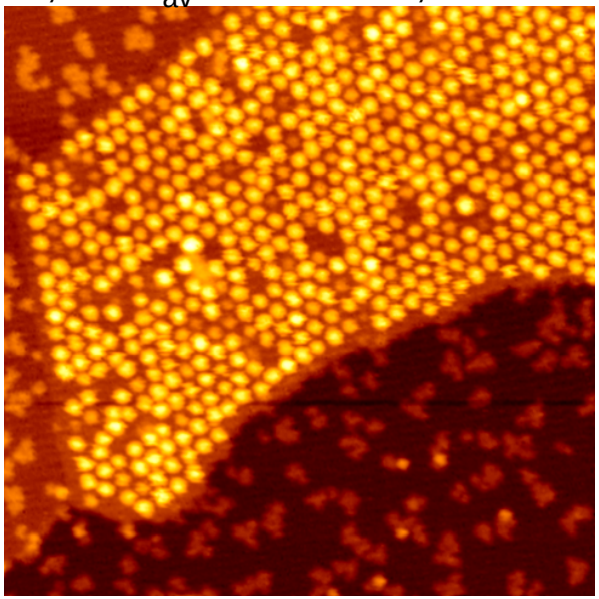

Re, $30 \leq s_{av} \leq 70$ atoms, 310 K

750 Å

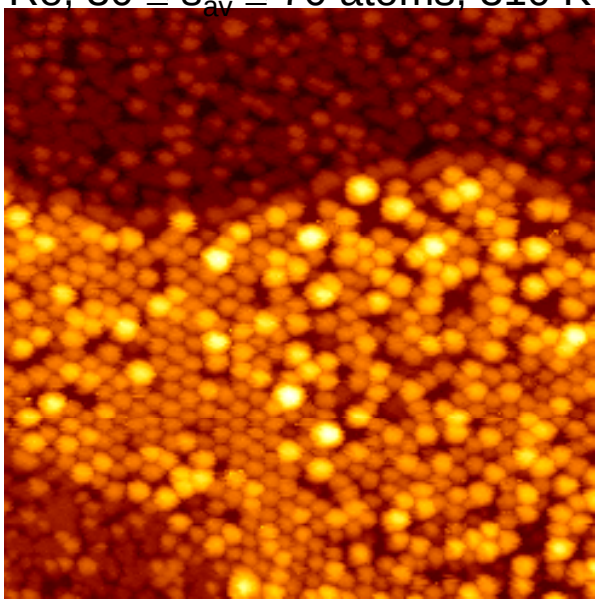

Ir, s_{av} = 70 atoms, 350 K

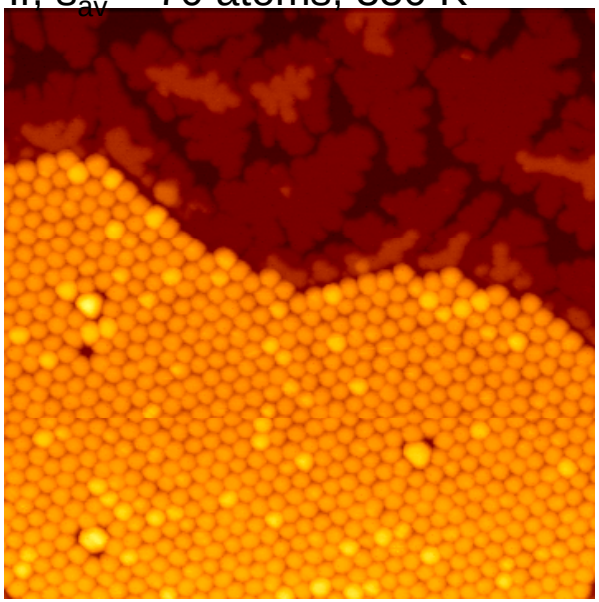

Fig. 5.24

Size Dependence of CO Oxidation by Pt-Clusters on MgO

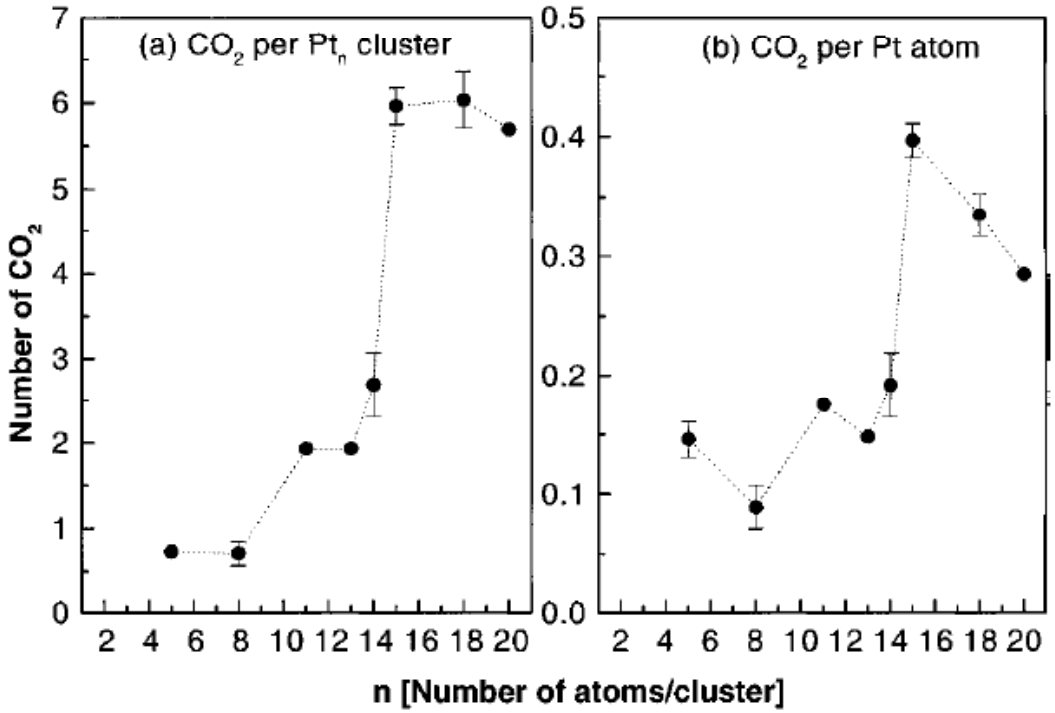

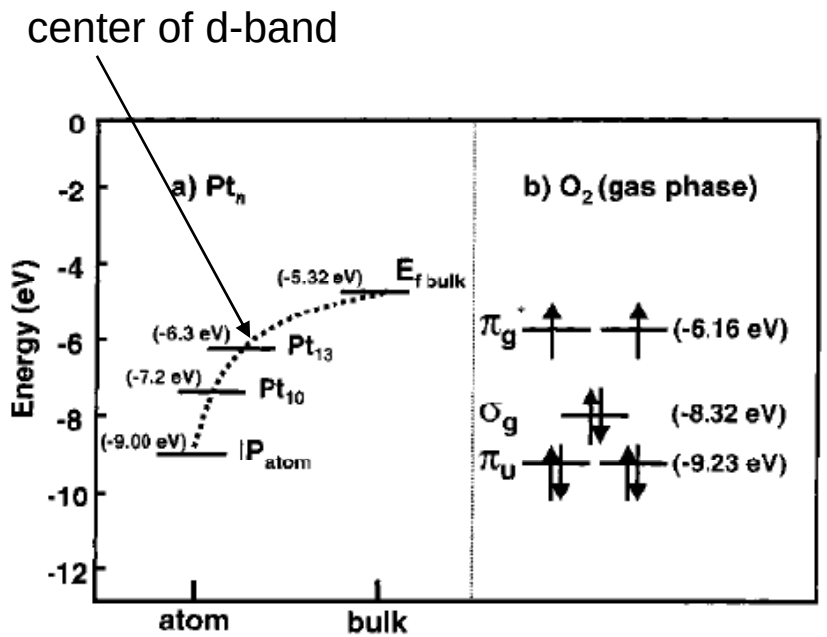

U. Heiz, A. Sanchez, S. Abbet, W.-D. Schneider, J. Am. Chem. Soc. 121 (1999) 3214

Fig. 5.25

Size Depence of CO Oxidation by Au-Clusters on TiO_2

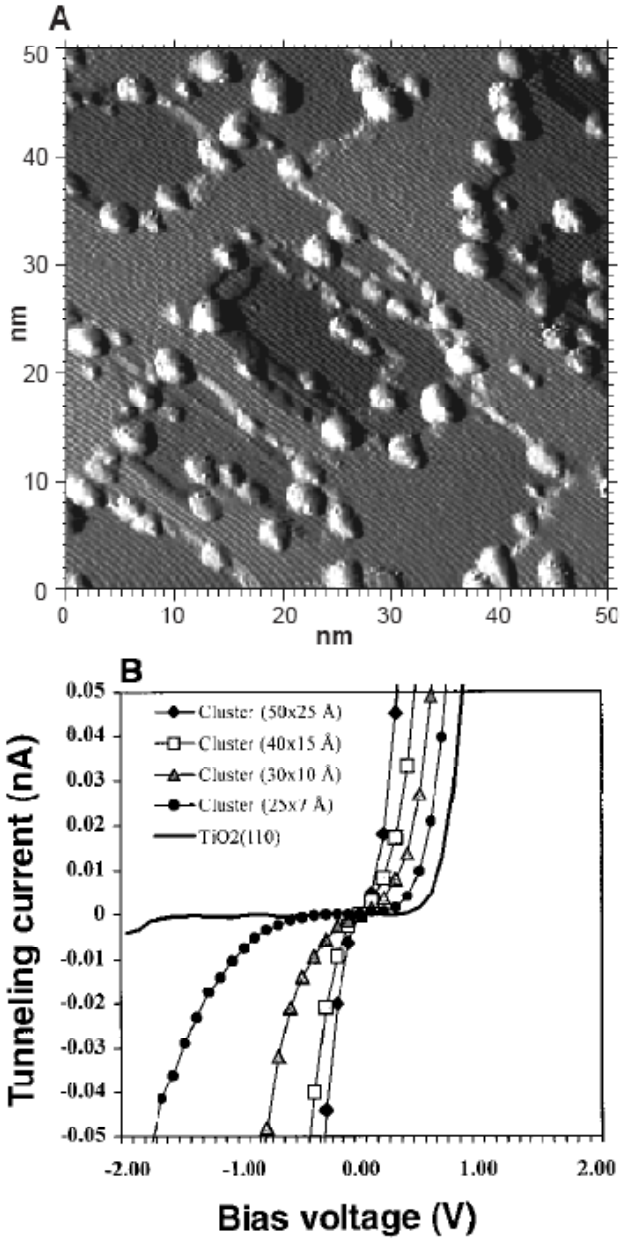

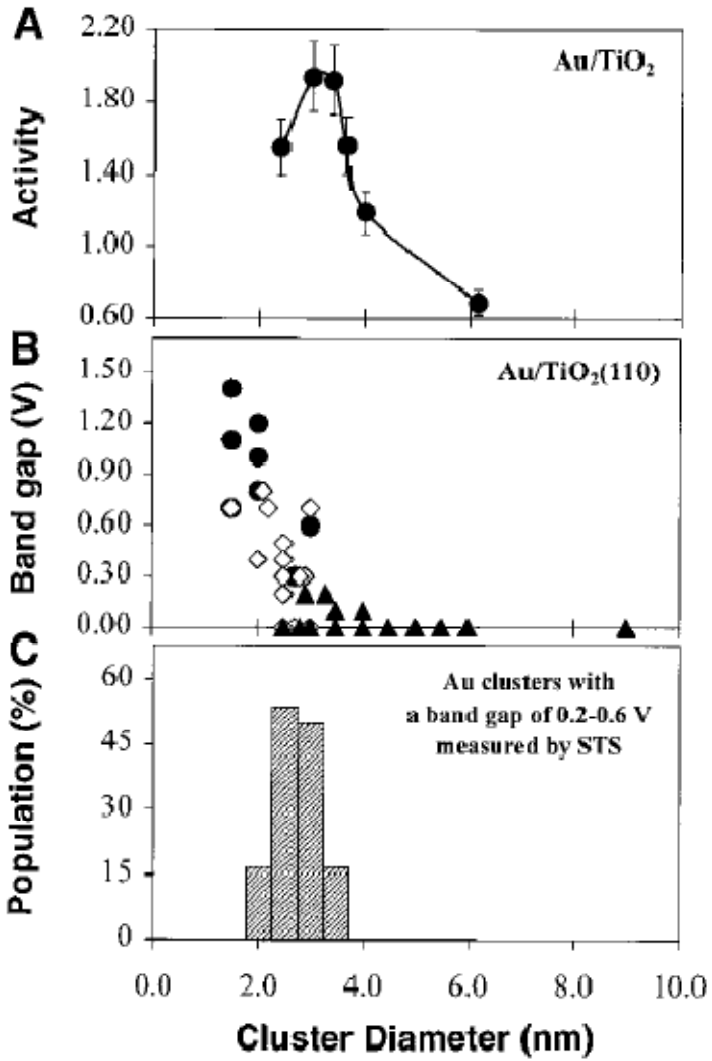

Fig. 3. (**A**) The activity for CO oxidation at 350 K as a function of the Au cluster size supported on $TiO_2(110)$-(1×1) assuming total dispersion of the Au. The $CO:O_2$ mixture was 1:5 at a total pressure of 40 Torr. Activity is expressed as (product molecules) × (total Au atoms)$^{-1}$ s^{-1}. (**B**) Cluster band gap measured by STS as a function of the Au cluster size supported on $TiO_2(110)$-(1×1). The band gaps were obtained while the corresponding topographic scan was acquired on various Au coverages ranging from 0.2 to 4.0 ML. (●) Two-dimensional (2D) clusters; (□) 3D clusters, two atom layers in height; (▲) 3D clusters with three atom layers or greater in height. (**C**) Relative population of the Au clusters (two atom layers in height) that exhibited a band gap of 0.2 to 0.6 V as measured by STS from $Au/TiO_2(110)$.

M. Valden, X. Lai, D.W. Goodman, Science 281 (1998) 1647

Fig. 5.26

Resistance of Au-Clusters to Oxidation by an O-Plasma

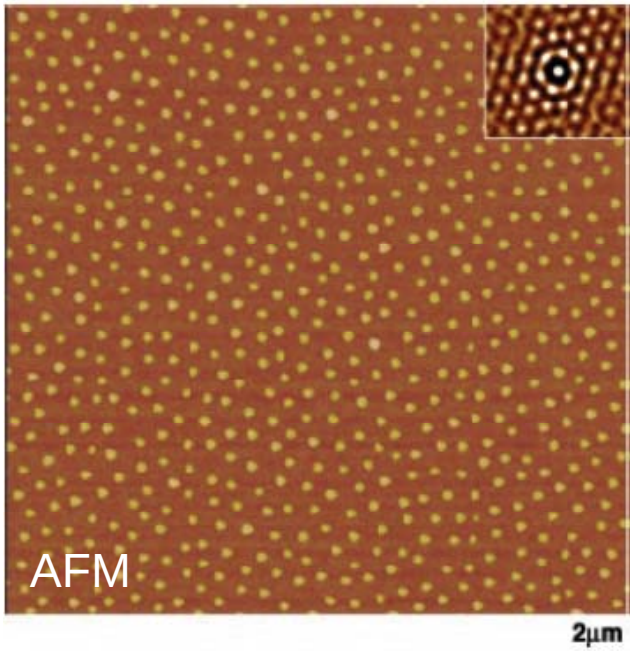

XPS of Au(111) treated in O plasma

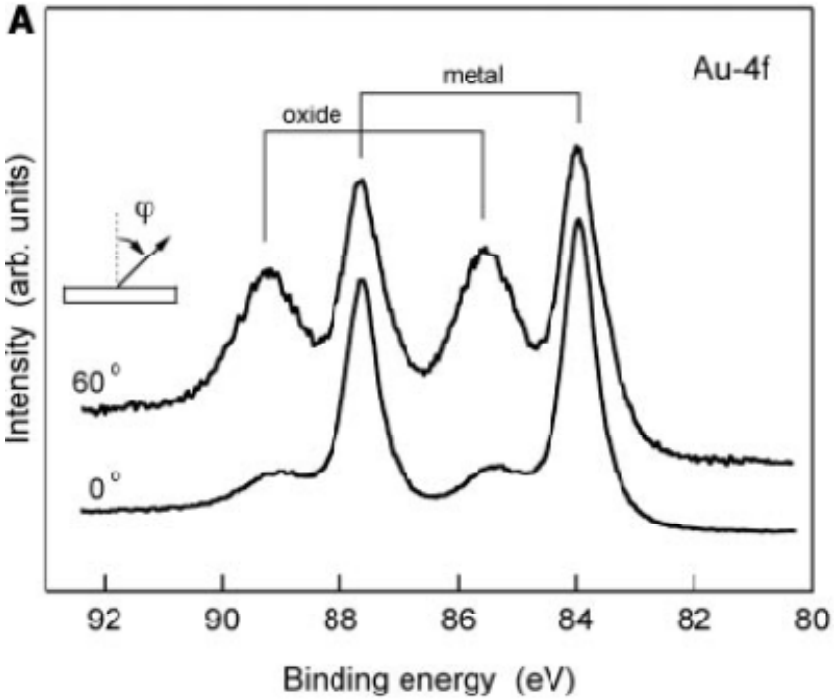

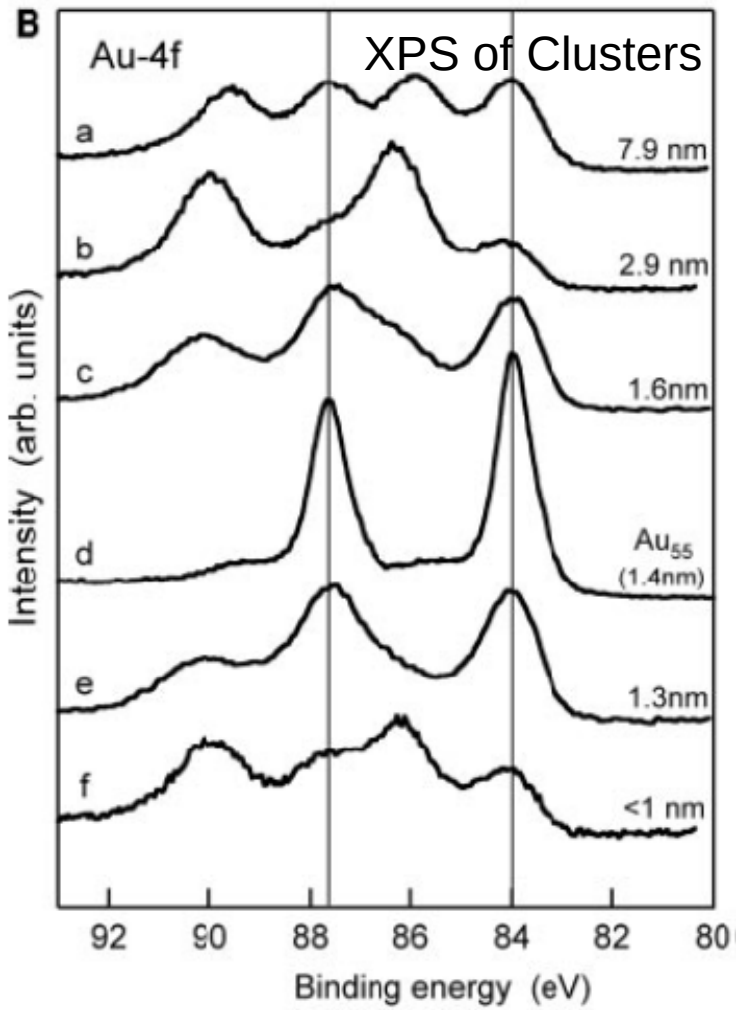

Fig. 5.27

H.-G. Boyen et al., Science 297 (2002) 1533

The Future of Magnetic Data Storage

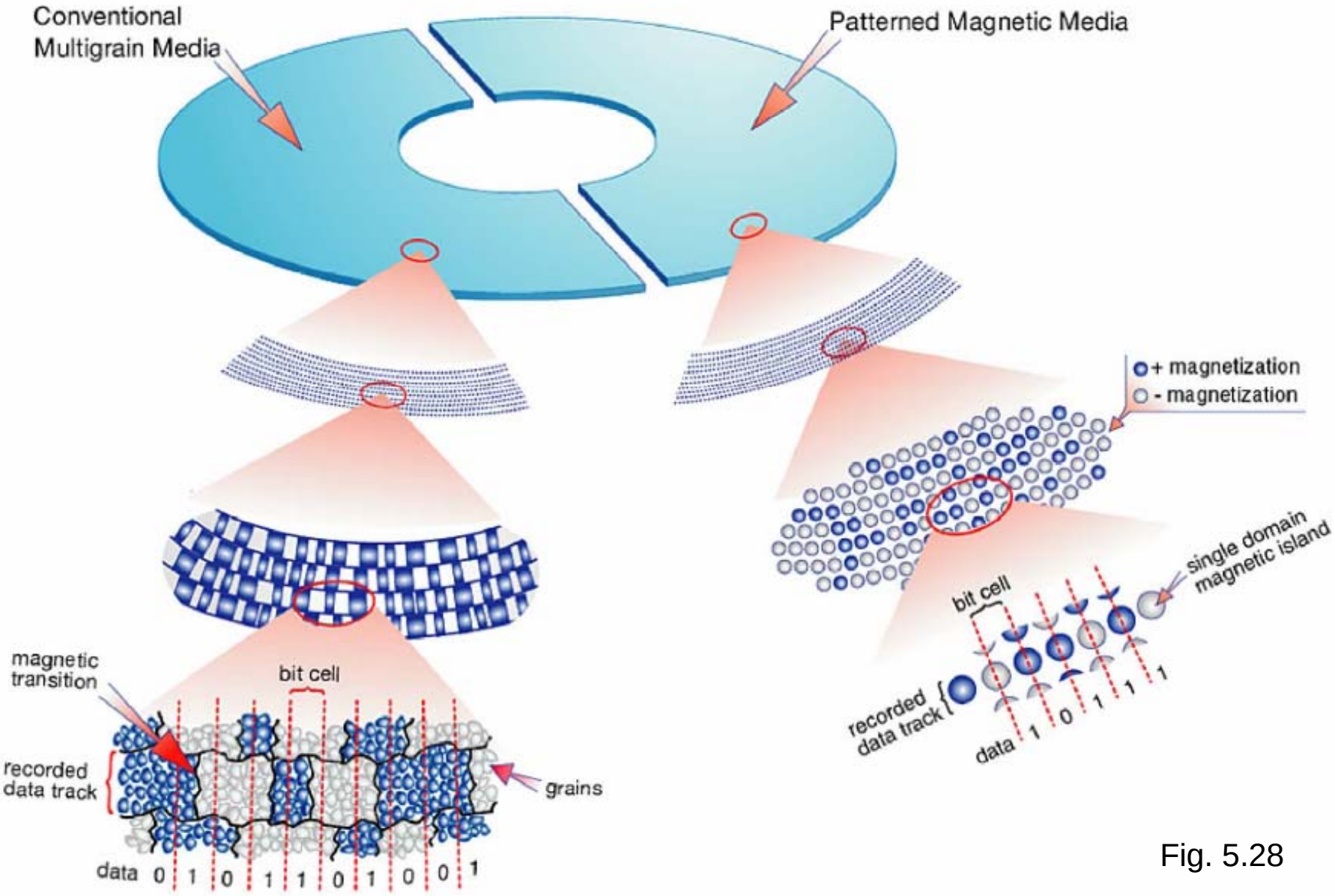

Fig. 5.28

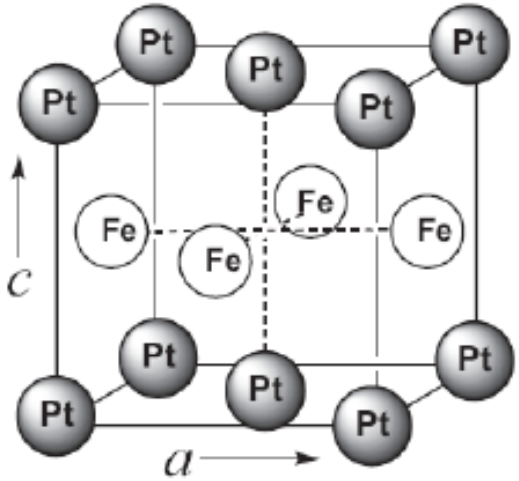

The FePt
$L1_0$-Phase

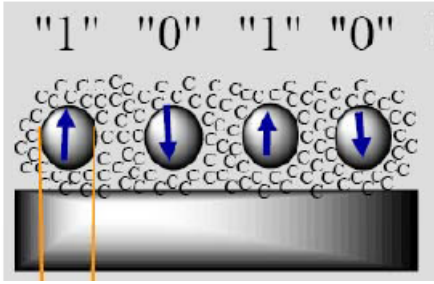

$Fe_{50}Pt_{50}$ nanoparticles in organic matrix

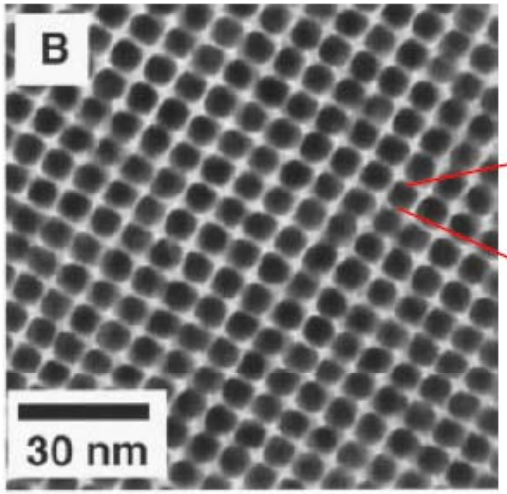

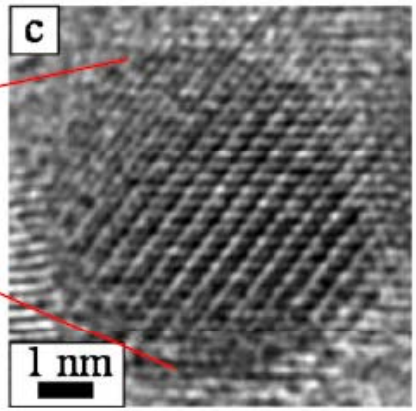

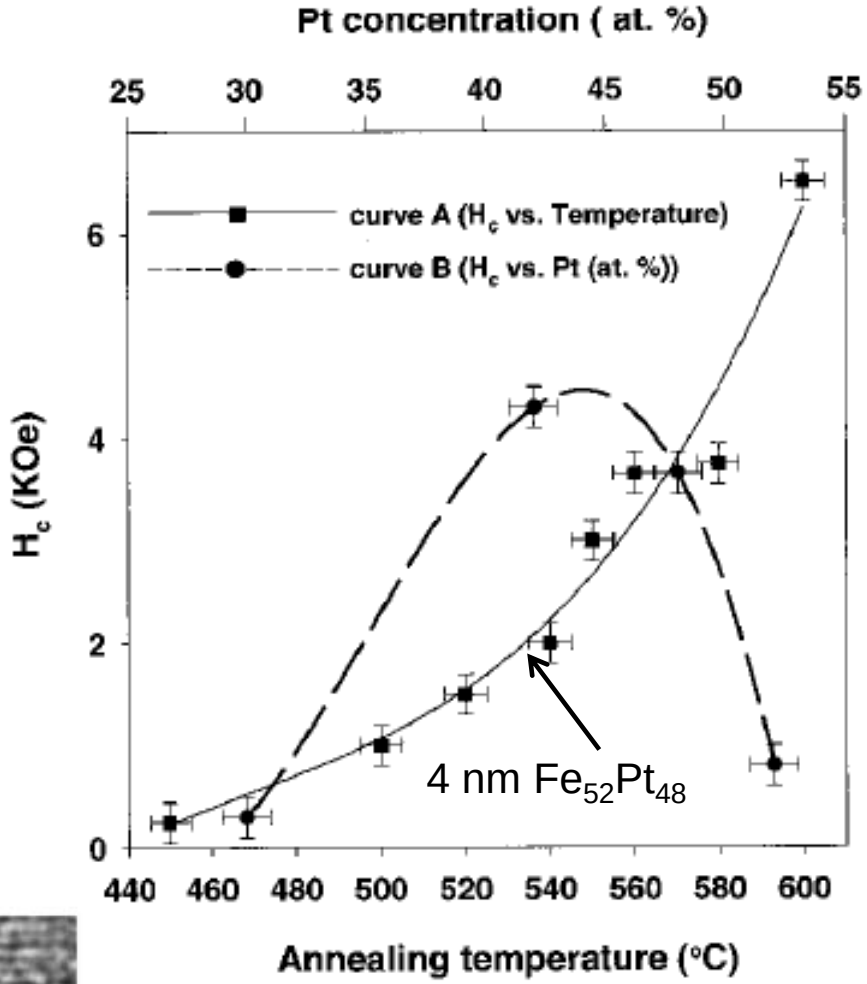

Fig. 5.29

Magnetization and Hysteresis in Dependence of Particle Size and Temperature for Co Clusters

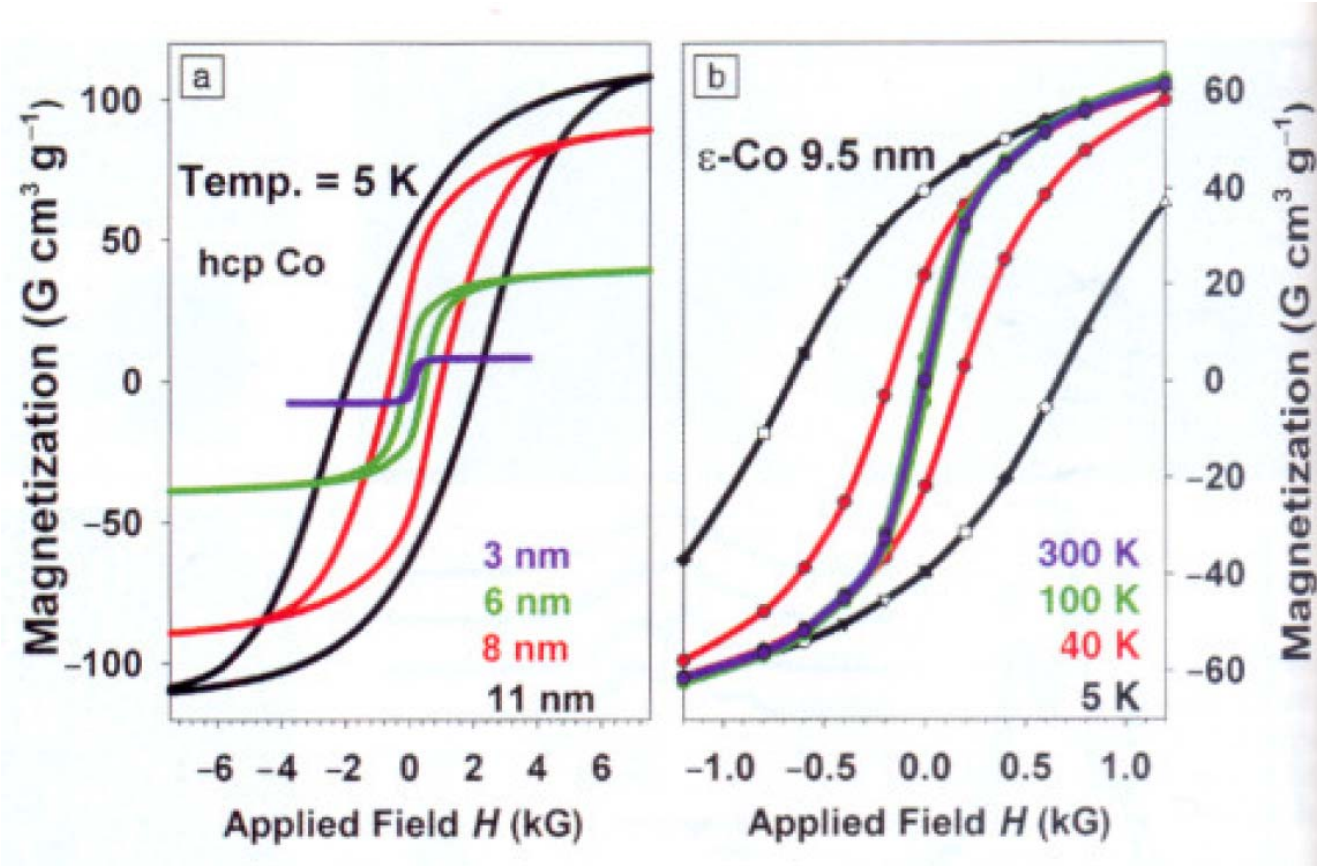

C.B. Murray et al. MRS Bulletin 26 (2001) 985

Fig. 5.30

Figures of Chapter 6: Epitaxy and Thin Films

Examples of Thin Film Applications

TiN hard-coating for steel cutting tools

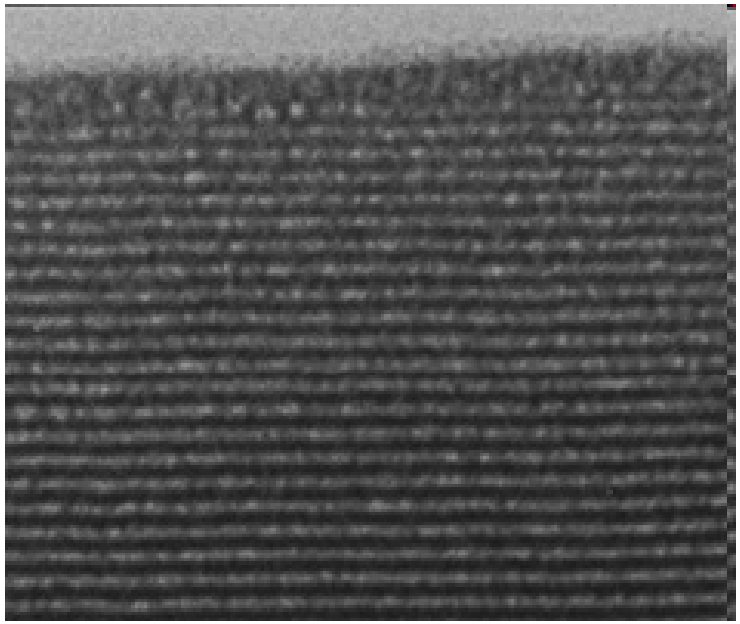

TEM of a W-Si X-ray mirror, periodicity 2.5 nm

Fig. 6.1

Examples of Thin Film Applications

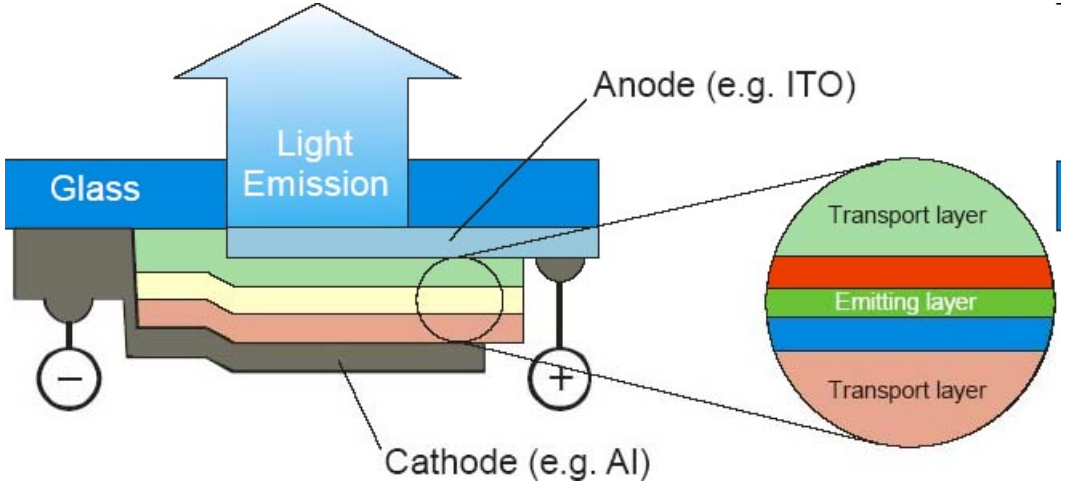

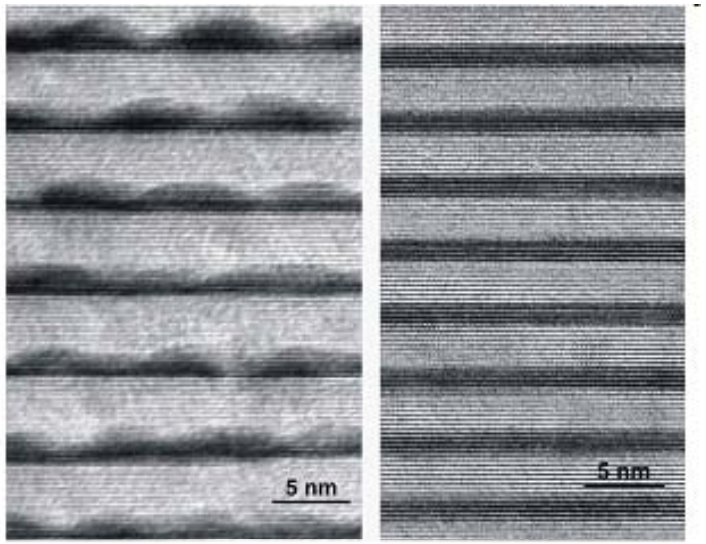

Figure 1: High-resolution transmission electron microscopy images of QD (left) and QW (right) superlattices for ISB absorption at 1.55 µm.

organic light emitting diode OLED

Fig. 6.2

Energy Minimizing Processes – Limited Mobility

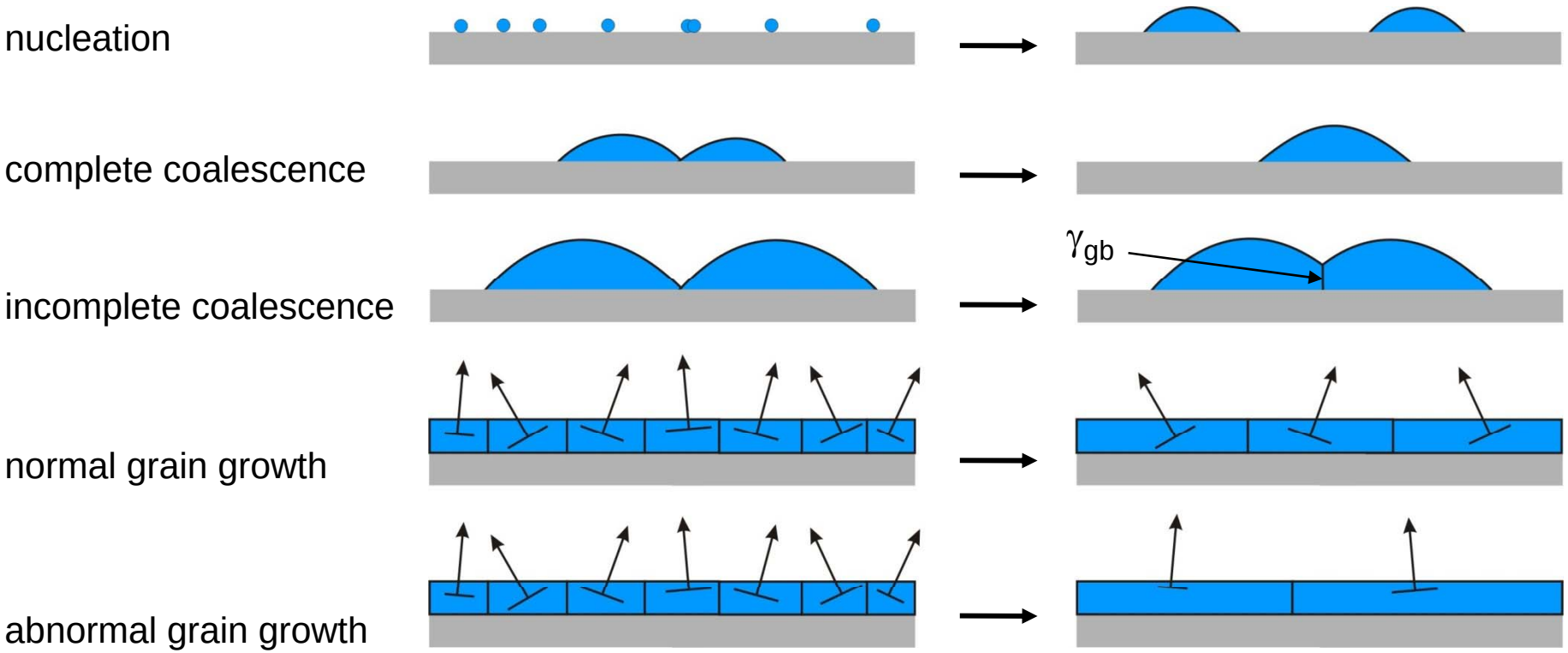

Fig. 6.3

Temperature Dependence of Thin Film Structure

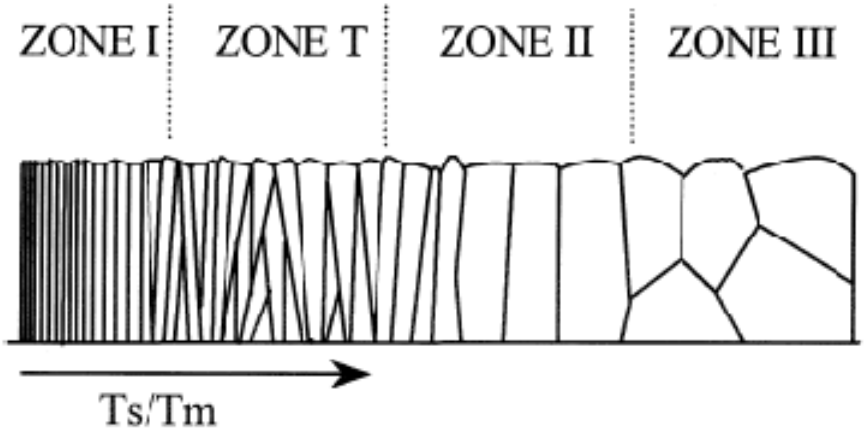

thin film growth in poor vacuum
(Thornton model)

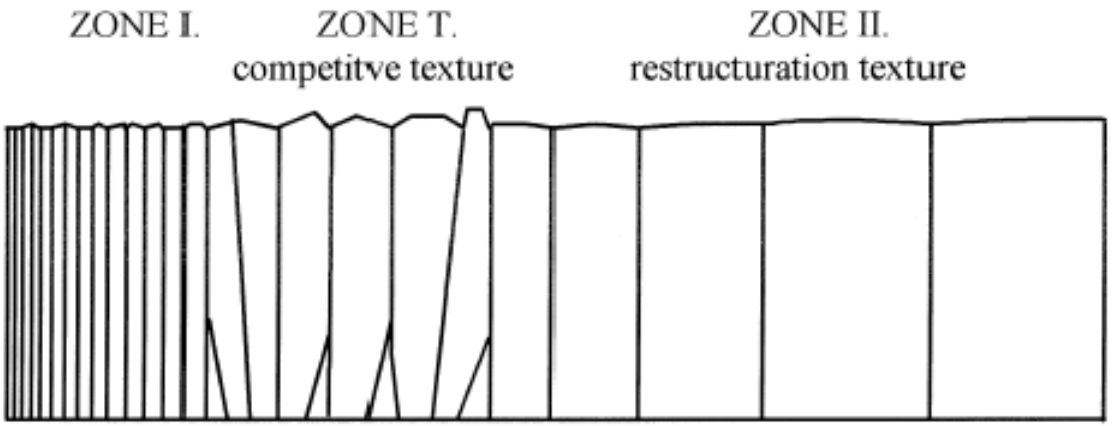

thin film growth in good vacuum
(Barna model)

P.B. Barna, M. Adamik, Thin Solid Films 317 (1998) 27

Fig. 6.4

Epitaxy of Rutile on Hematite

Fig. 6.5

Epitaxial Relation for Rutile on Hematite

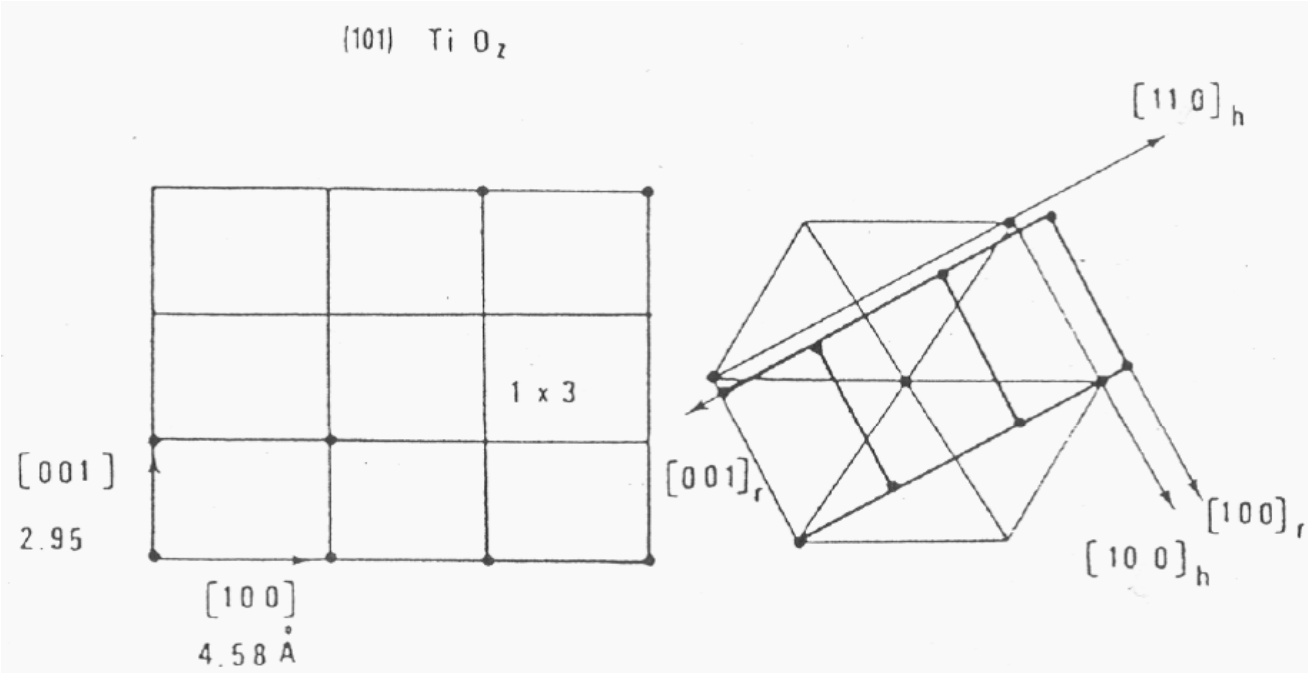

Species	Rows	Å	Misfit %
Fe_2O_3	[11 0] x 1	5.04 x $\sqrt{3}$	-3
	[10 0] x 1	5.04	
TiO_2	[001] x 3	2.95 x 3	+10
	[100]	4.58	

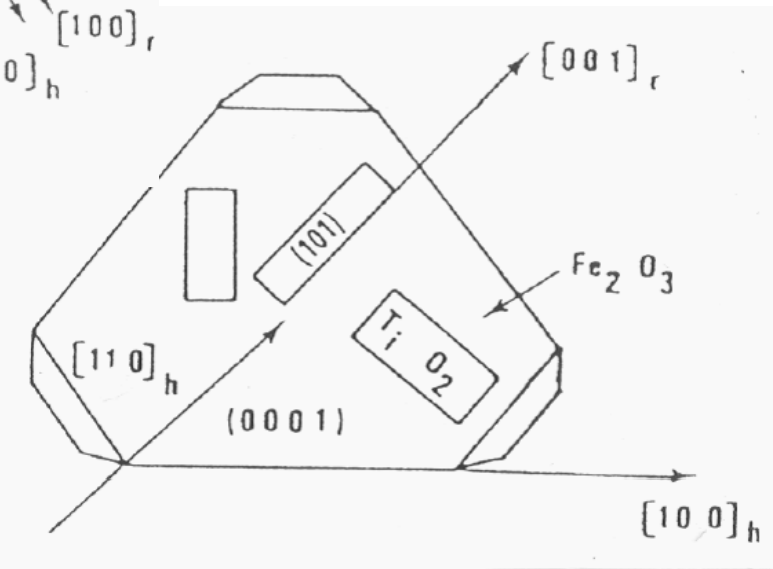

Fig. 6.6